Cellulose (2019) 26:2425–2435
https://doi.org/10.1007/s10570-019-02254-x

ORIGINAL RESEARCH

A comparative study on the starch-based biocomposite films reinforced by nanocellulose prepared from different non-wood fibers

Qifeng Chen · Yayun Liu · Guangxue Chen

Received: 28 June 2018 / Accepted: 5 January 2019 / Published online: 9 January 2019

Abstract Nanocellulose was extracted from three kinds of non-wood fibers (bamboo, cotton linter, and sisal) by TEMPO-mediated oxidation and high pressure homogenization. Starch-based composite films containing different kinds of nanocellulose with different content (0–10 wt%) were prepared via solution casting method. The morphology and structure of the three kinds of nanocellulose and their respective effects on the composite films were compared by various characterizations. The impacts of nanocellulose content on the thermal stability and mechanical properties of the composite films were also evaluated. The study found that morphology and chemical composition of the nanocellulose obtained from different sources were almost the same, but there were slight differences in their size and crystallinity. Bamboo nanocellulose had the highest aspect ratio, which enabled it to provide the greatest reinforcing effects on the mechanical properties and barrier properties of the composite films. The addition of nanocellulose improved the mechanical properties of the films but reduced their elongation at break and thermal stability. This study paves the route for choosing the most effective non-wood nanocelluloe source and mixed ratio to produce food packaging with the best performance.

Q. Chen · Y. Liu · G. Chen (✉)
State Key Laboratory of Pulp and Paper Engineering,
South China University of Technology,
Guangzhou 510640, China
e-mail: qfchen@scut.edu.cn

Graphical abstract

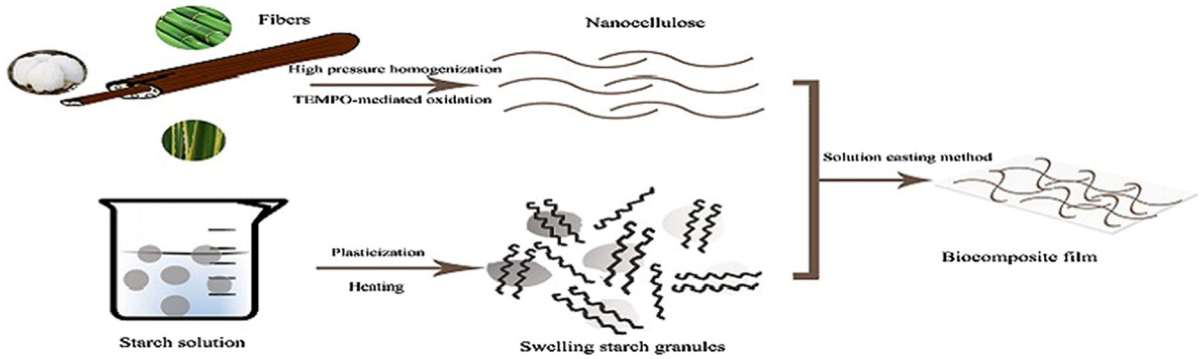

Keywords Nanocellulose · Starch · Biocomposite films · Green packaging

Introduction

In recent years, growing ecological problems and energy requirements have made it necessary to develop bio-based packaging materials with excellent performance and environmental friendliness (Li et al. 2015). Among the many bio-polymers, starch has become one of the most attractive alternatives to petroleum-based plastic packaging due to its lower cost, richer yield and biodegradability (Carvalho 2008). Studies have found that starch-based materials reduced the utilization of non-renewable resources and the impact of synthetic plastics on the environment (Bonilla et al. 2013). However, the low water resistance and high brittleness of starch films limit its widespread use (Zhao et al. 2006). One of the effective ways to improve these weaknesses is to add plasticizing compounds and other polymers (Peressini et al. 2003).

Nanocellulose generally refers to a cellulosic material that has at least one dimension in the nanometer range (Abdul Khalil et al. 2014). Compared with natural cellulose, nanocellulose has a higher crystallinity, surface area, mechanical strength and energetically active sites, and presents enormous development potential in food packaging, pharmaceuticals, biomedicine and other fields (Faradilla et al. 2016). The incorporation of biodegradable biomass nanofibers such as cellulose nanofibers with other polymers has been proven an important strategy for obtaining nanocomposites with higher mechanical properties (Khalil et al. 2012; Montero et al. 2016). Nanocellulose has been successfully used to develop biocomposite films and high strength specialty paper (Babaee et al. 2015; Tabarsa et al. 2017). Compared to pure thermoplastic starch films, nanocellulose obtained from non-wood raw materials such as wheat straw was also found to increase the barrier property of the nanocomposite films (Kaushik et al. 2010).

Most of the literatures focus on studying the effects of different preparation process and content of nanocellulose on the starch film (Zhou et al. 2012; Karimi 2014; Santana et al. 2016). However, the geometric properties (shape, length and diameter) of nanocellulose structure depend not only on the extraction process but also on the cellulose source (Deepa et al. 2015). The nanocellulose prepared from different sources has different reinforcing effects on the starch film. It is of great significance to systematically compare the reinforcing effects of nanocellulose prepared from different raw materials on the starch film for selecting the best packaging material.

In this study, three types of nanocellulose were prepared from three kinds of non-wood fiber (bamboo, cotton linter, and sisal) by TEMPO-mediated oxidation and high pressure homogenization. The basic properties of nanocellulose prepared from different raw materials were discussed and compared through transmission electron microscopy, atomic force microscopy, X-ray diffraction and fourier transform infrared spectroscopy. Moreover, three kinds of nanocellulose were respectively blended with the starch to form a composite film, and then three types of composite films containing the best ratio of nanocellulose were obtained by changing the

nanocellulose content. The reinforcing effects of nanocellulose sources on starch-based films were evaluated by scanning electron microscopy, thermogravimetric, universal testing machine, gas permeability tester, and moisture permeability tester. Results of this study could help us choose the most suitable raw materials and mixed ratio to prepare green packaging materials.

Materials and methods

Materials

Nanocellulose was extracted from three kinds of non-wood fibers (Bamboo, cotton linter, sisal). Sodium bromide (NaBr) and 2,2,6,6-tetramethylpiperidine-1-oxyl (TEMPO) were purchased from shanghai Aladdin Biochemical Co., Ltd (Shanghai, China). Corn starch (CS) (amylose content: 32.5 ± 0.3%), sodium hypochlorite (NaClO), sodium hydroxide (NaOH) and glycerin ($C_3H_8O_3$) were obtained from Sinopharm Chemical Reagent Co., Ltd (Beijing, China). All the chemicals were reagent grade and used without further purification.

Preparation of nanocellulose from different raw material

The wet pulp corresponding to 10 g dry weight was soaked in the appropriate amount of deionized water overnight and fully separated by mechanical stirring at 320 rpm. Next, 0.16 g TEMPO and 1 g sodium bromide were mixed with the slurry. Then 100 mL sodium hypochlorite was gradually added into the slurry with continuous stirring at the pH range of 10–10.5 adjusted by 0.5 M sodium hydroxide solution. When the pH of the solution was no longer changed, the reaction was stopped by adding 1 mL ethanol. After the reaction was completed, the slurry was suctioned and washed repeatedly at least three times until the chemical was completely removed. Finally, the oxidized pulp was homogenized by a high pressure homogenizer (NOOZLE Mini, China) at 180 MPa for 8 cycles to obtain gelatinous nanocellulose. The obtained nanocellulose prepared from bamboo, cotton linter, and sisal was abbreviated as BNC, CNC, and SNC respectively in the following description.

Preparation and optimization of nanocellulose-starch composite film

The mixture of 5 g starch and 1.5 g glycerol were added to 100 mL deionized water. Afterwards, the solution was placed in an oil bath at a constant temperature of 80 °C and a stirring speed of 300 rpm for 30 min. After the plasticization was completed, the film-forming solution was divided into six parts, and then were respectively incorporated with different nanocellulose content (0–10 wt%, accounted for in the weight of CS) to produce nanocomposite film. The film-forming solution was degassed under a vacuum of 0.01 MPa for 15 min to remove bubbles in the solution. Finally, the solutions with different nanocellulose content were casted on PTFE plates and dried in an oven at 40 °C (Fig. 1).

Characterization methods

Transmission electron microscopy (TEM)

After sonicated with ice bath (5 min) and diluted to 100 μg/mL, the nanocellulose suspension was deposited on a copper grid and stained with a 3% acetic anhydride, and then dried at room condition. The microscopic morphology and particle size were observed using a JEM-1400Plus (Bruker) transmission electron microscope operated at 120 kV.

Atomic force microscopy (AFM)

Surface topography and morphology of the samples were analyzed using an atomic force microscope (Bruker Multimode 8, Germany). Silicon cantilevers with a typical resonant frequency of 240 kHz and spring constant of 40 N/m were used to acquire images in tapping mode at room temperature under ambient conditions. The scanning rate was around 1 Hz.

X-ray diffraction (XRD)

X-ray diffraction patterns were recorded for the pellets prepared from freeze-dried nanocellulose with an X-ray diffractometer (Bruker VERTEX 70, Germany), equipped with Cu Kα radiation source (wavelength = 0.154 nm) operating at 40 kV and 40 mA.

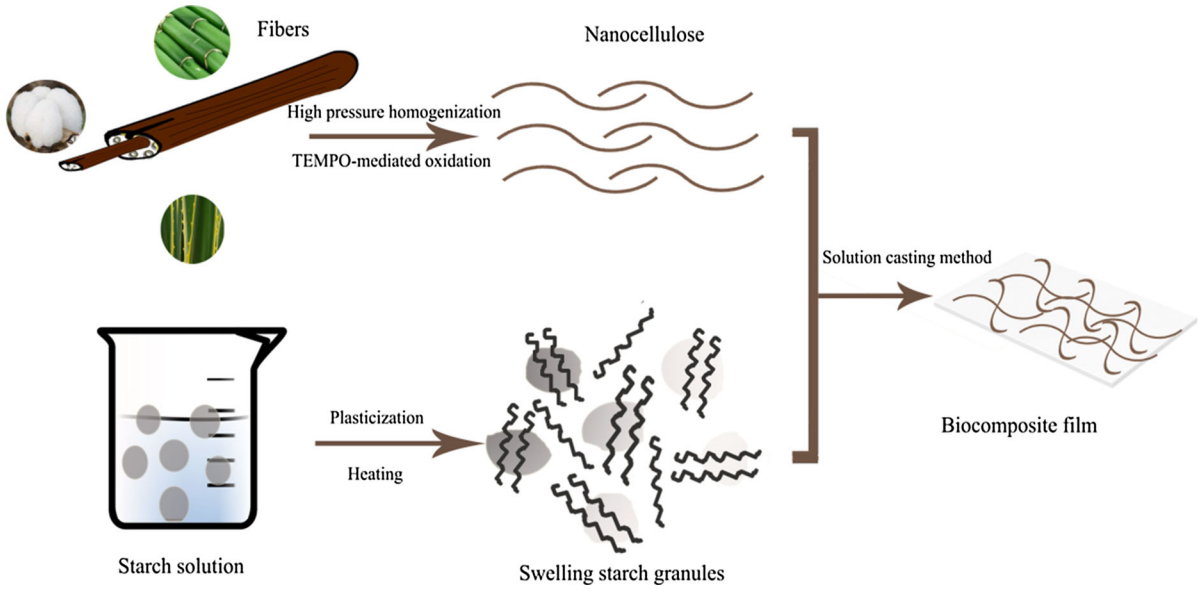

Fig. 1 Preparation process of starch-based biocomposite films reinforced by nanocellulose

The XRD patterns were recorded over the angular range 2θ = 5°–40°.

Crystallinity index for nanocellulose was calculated according to the Segal method (Segal et al. 1959) as shown in Eq. 1.

$$\text{Crystallinity index } (\%) = \frac{I_{200} - I_{am}}{I_{200}} \times 100 \qquad (1)$$

where I_{200} is the maximum intensity of the diffraction peak at around 2θ = 22.5° corresponding to (200) planes, I_{am} is the intensity of the diffraction at around 2θ = 18°, representing the amorphous fraction for cellulose I (French 2014).

Fourier transform infrared spectroscopy (FTIR)

Spectral analysis of the sample was performed by a Fourier Transform Infrared Spectrometer (Bruker VERTEX 70, Germany) with the wavelength ranging from 400 to 4000 cm^{-1} and a spectral resolution of 4 cm^{-1}.

Scanning electron microscopy (SEM)

The surface morphology of nanocomposites was observed using a scanning electron microscope model (Hitachi SU8220, Japan) with an accelerating voltage of 10–20 kV.

Thermogravimetric analysis (TGA)

The thermal stability of samples was tested by a thermogravimetric analyzer (TA Q500, American) under a N2 atmosphere, at the temperature ranging from room temperature to 600 °C and a heating rate of 20 °C/min.

Tensile tests

The film was cut into rectangular strips in the size of 8 mm * 60 mm and placed in a constant temperature and humidity environment (23 °C, 50% relative humidity) for more than 48 h to balance the moisture content. The thickness of each strip was then tested using a micrometer (L&W 251, Sweden), and the mechanical properties were evaluated by a universal testing machine (INSTRON 5565, American) with a test speed of 20 mm/min and an initial gap of 20 mm. Three replicate measurements were conducted and the averages were reported.

Water vapour permeability (WVP) and Oxygen permeability (OP)

The moisture content of the film was firstly balanced as mentioned before. Then the water vapour permeability (WVP) and oxygen permeability (OP) were

separately tested using a gas permeability tester (VAC-VI, China) and a moisture permeability tester (TSY-TIH, China) in accordance with the ASTM standard E96 and D1434.

Results and discussion

Morphology analysis of nanocellulose

Figure 2 shows the TEM images of the nanocellulose isolated from bamboo, cotton linter, and sisal respectively. The nanocellulose prepared from different raw materials exhibited a complex, highly-entangled and web-like structure as reported in other researches (Xu et al. 2013; Sacui et al. 2014). Kinks were partly observed, indicating that the nanocellulose experienced some mechanical damage (Saito et al. 2007). Among them, the nanocellulose obtained from bamboo pulp and cotton pulp had slender fibrillation morphology, while the nanocellulose prepared from sisal pulp appeared to have shorter length and greater width.

From the AFM images shown in Fig. 3, it can be seen that the nanocellulose was in the form of a curved winding filament with good dispersibility. The average lengths of the nanocellulose extracted from bamboo, cotton linter, and sisal were 755 ± 435, 635 ± 455 and 464 ± 326 nm respectively. The widths of the three samples ranged from 5 to 14 nm depending on the source. The apparent size was slightly larger than the actual value due to the AFM tip convolution. Some short nanocellulose could be observed due to the high NaClO addition level used in the oxidation stage, which resulted in a remarkable depolymerization of cellulose chains (Shinoda et al. 2012, Shimizu et al. 2014). The size measurements from AFM images showed that there would be some variation in fiber size for different sources. The aspect ratio of BNC and SNC were the highest and the lowest respectively, in agreement with that observed in the TEM.

Structural analysis of nanocellulose

XRD patterns of original fibers and nanocellulose are shown in Fig. 4a, b. In all cases, the original cellulose I crystal structure was maintained in the nanocellulose. The peak observed as one broad peak around 15°–16° was actually a combination of two peaks corresponding to (1-10) and (110) planes. The peaks at $2\theta = 22.5°$ and 34.5° corresponded to the (200) and (004) crystallographic planes (French 2014). As previously stated (French and Santiago Cintrón 2013), the main contributors of intensity to the three main peaks had Miller indices of (1-10), (110) and (200). Therefore, it was confirmed that the preparation of nanocellulose by TEMPO-mediated oxidation could protect the crystalline structure well, and the oxidation mainly took place in the amorphous region of cellulose. However, the crystallinity index of the nanocellulose prepared from different sources had an obvious decrease compared with that of the original fibers. It was likely that a high shearing action during the homogenization process may resulted in damage either through breaking effect or peeling-off of the cellulose chains on the surface of the crystallite (Besbes et al. 2011). The crystallinity index was of the order SNC > CNC > BNC, this order agrees with the crystallinity index of the three original fibers. It was concluded that the differences in crystallinity of the nanocellulose depended on the cellulose raw materials under the same experimental condition (Table 1).

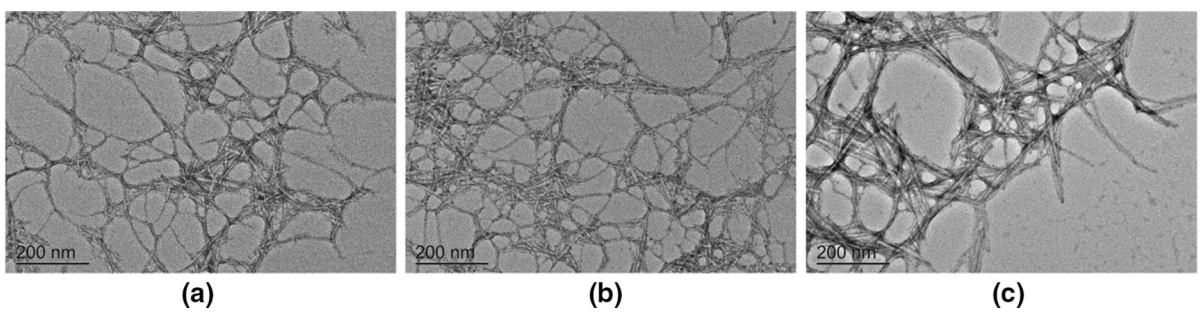

Fig. 2 TEM images of nanocellulose obtained from **a** bamboo, **b** cotton linter and **c** sisal

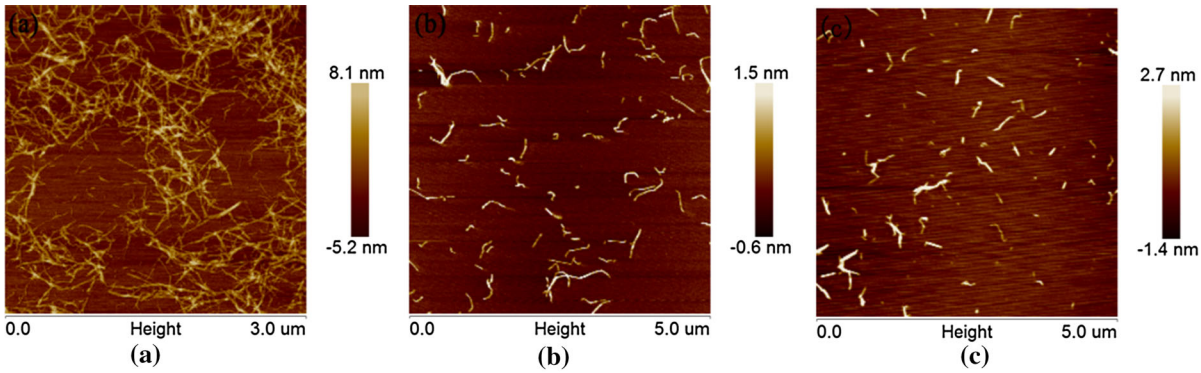

Fig. 3 AFM images of nanocellulose obtained from **a** bamboo, **b** cotton linter and **c** sisal

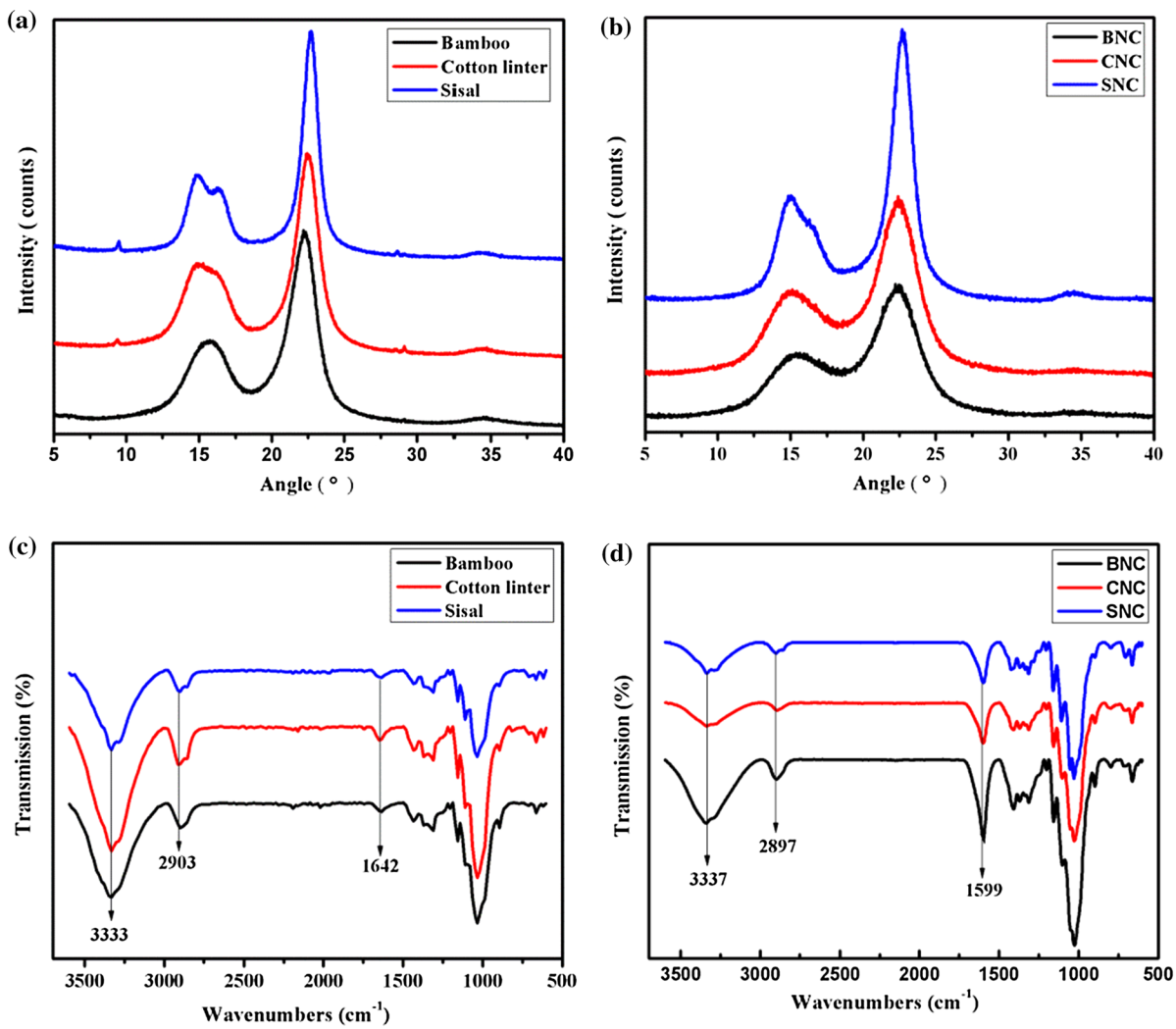

Fig. 4 XRD patterns and FTIR spectra of three kinds of original fibers (**a**, **c**) and corresponding nanocellulose (**b**, **d**)

Table 1 XRD analysis parameters for crystallinity index of the nanocellulose isolated from various sources

Sample	Crystallinity index (%)
Bamboo	78.2
Cotton linter	82.7
Sisal	89.3
BNC	60.1
CNC	66.5
SNC	83.9

Figure 4c, d show the FTIR spectra of the untreated fibers and nanocellulose obtained from bamboo, cotton linter and sisal respectively. The absorption band observed in the FTIR spectra of all the samples (original fibers and nanocellulose fibers) within 3400–3300 cm^{-1} was assigned to the O–H stretching vibrations of the hydroxyl group (Chirayil et al. 2014). All the samples also exhibited a typical absorption band around 2900 cm^{-1} corresponding to the stretching vibrations of C–H groups. The peak at 1642 cm^{-1} in original fibers was associated to the O–H bending of the adsorbed water (Mandal and Chakrabarty 2011). The most important change was the appearance of the carbonyl groups (C=O) stretching band at 1599 cm^{-1} in nanocellulose fibers, which was attributed to sodium carboxylate groups (–COONa) (Max and Chapados 2004; Jiang and Hsieh 2015), indicating that the hydroxyl groups at the C6 position of cellulose molecules were successfully converted to sodium carboxylate. The result showed that there was no significant difference in the infrared spectrum of nanocellulose extracted from different sources.

Morphology analysis of nanocomposites

The SEM diagrams of microcrystalline cellulose composite films were shown in Fig. 5. The surface of the starch-based films was smooth, indicating that the starch plasticized under the action of the glycerol. As a whole, 10 wt% nanocellulose were dispersed uniformly in the composite film, while an agglomeration of nanocellulose occurred only in individual regions of the starch film. All the nanocellulose in the films intertwined to form a network structure and the compatibility is good. Observation of images from Fig. 6 showed that surface of the composite film containing different kinds of nanocellulose seem to be no difference and all have a good light transmittance.

Thermal stability analysis of nanocomposites

Figure 7a, b show the thermogravimetric curves of composite films reinforced with 4 wt% nanocellulose from different sources, their trends were roughly the same. The decomposition of all the composite films was mainly divided into three stages. The first stage occurred below 220 °C, mainly attributed to the evaporation of water. The second stage was between 220 and 340 °C, at this stage, the weight of the film decreased rapidly, mainly due to the decomposition of starch and nanocellulose in the film. The third stage, which appeared above 340 °C, was caused by the decomposition of residual materials in the film. The thermal decomposition temperatures of the composite films with different types of nanocellulose were about the same, but there were some differences in the maximum thermal decomposition rate and weight loss rate. The maximum thermal decomposition rate and weight loss rate of BNC/CS composite film was the smallest.

Figure 7c, d show the thermogravimetric curves of composite films reinforced with different nanocellulose content. As the concentration of nanocellulose in the composite films increased, the decomposition temperature gradually decreased, indicating that nanocellulose reduced the thermal stability of the film. A possible explanation for this was that the flexibility of amylopectin chains decreased when crystalline cellulose was present (Kaushik et al. 2010). Another reason may be that glycerin accumulated on the surface of cellulose nanofibrils due to its higher affinity for the cellulose surface (And and Dufresne 2008); the accumulation of plasticizers in the cellulose/pullulan interface region improved the ability of amylopectin chains to crystallize, resulting in the formation of possible crystalline regions around the fibrils.

Mechanical properties analysis of nanocomposites

The tensile strength and the elongation at break of the composite films with different contents of BNC, CNC, and SNC respectively are shown in Table 2. Overall, the tensile strength of the composite film containing nanocellulose was greatly improved in comparison to

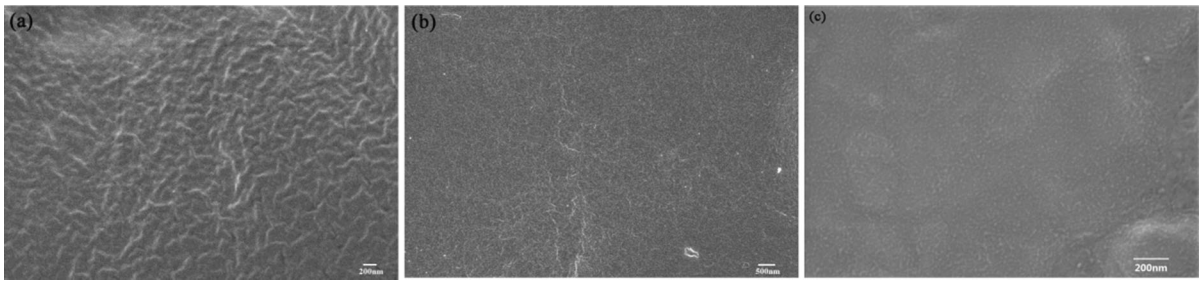

Fig. 5 SEM images of the starch films reinforced with 10 wt% nanocellulose prepared from: **a** bamboo, **b** cotton linter, **c** sisal

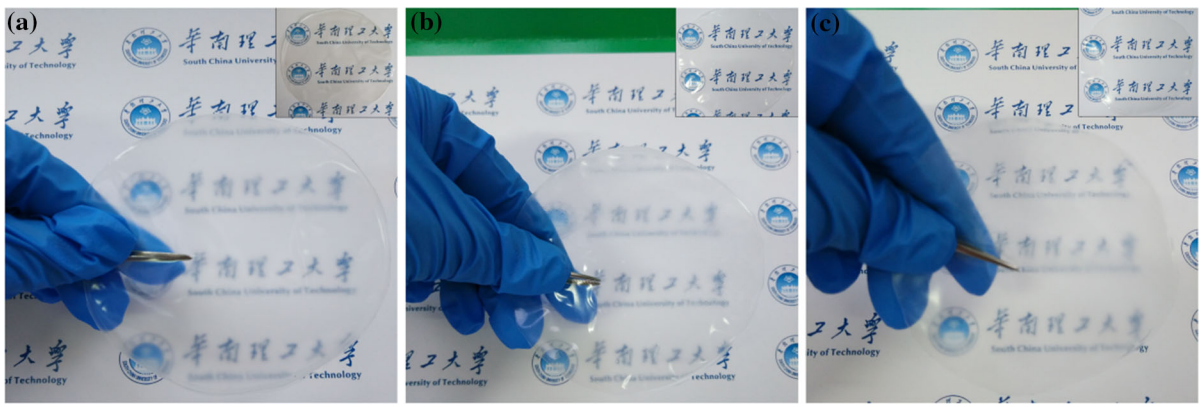

Fig. 6 Digital image of the starch films reinforced with 10 wt% nanocellulose prepared from: **a** bamboo, **b** cotton linter, **c** sisal

the pure starch film. However, the tensile strength did not gradually increased with the increasing nanocellulose content; it remained unchanged or even weakened after reaching maximum value. This may be because large amount of nanocellulose reduced its interaction with the polymer matrix, thereby reducing the strength of the composite film. In addition, high concentration of nanocellulose tended to agglomerate, resulting in an uneven stress distribution in the film (Savadekar and Mhaske 2012). The elongation at break gradually decreased with the increase of nanocellulose content. The reason is that the rigid network formed by nanocellulose and starch restricted the movement of the starch molecular chain and reduced the elongation at break (Chen et al. 2017).

By comparing the mechanical properties of starch films with nanocellulose extracted from different sources, BNC was found to provide the highest reinforcing mechanical strength for the composite film, followed by CNC, and finally SNC. This may be due to the largest aspect ratio of bamboo nanocellulose as observed in electron microscopy. From this result, it can be inferred that the aspect ratio of nanocellulose may have a greater effect on the strength of the composite film than the crystallinity of nanocellulose.

Barrier properties analysis of nanocomposites

The water vapor permeation and oxygen permeation of the starch-based composite film containing 4 wt% nanocellulose were shown in Fig. 8. Comparing to the pure starch film, the water vapor permeation of the composite film added with BNC, CNC, SNC was decreased by 27.60%, 21.98%, and 18.91% respectively, and the oxygen permeation decreased by 32.9%, 23.68%, and 15.35% respectively. This is because nanocellulose formed crystalline domains with a high degree of orientation in the film, allowing the transmission path of water vapor and oxygen to be extended (García et al. 2010; Kaushik and Kaur 2016), thereby reducing the amount of water vapor and oxygen per unit time. In addition, the water vapor permeation and oxygen permeation of the composite films containing BNC were the smallest. This result can be well understood because BNC had the largest length and formed a denser network structure, which

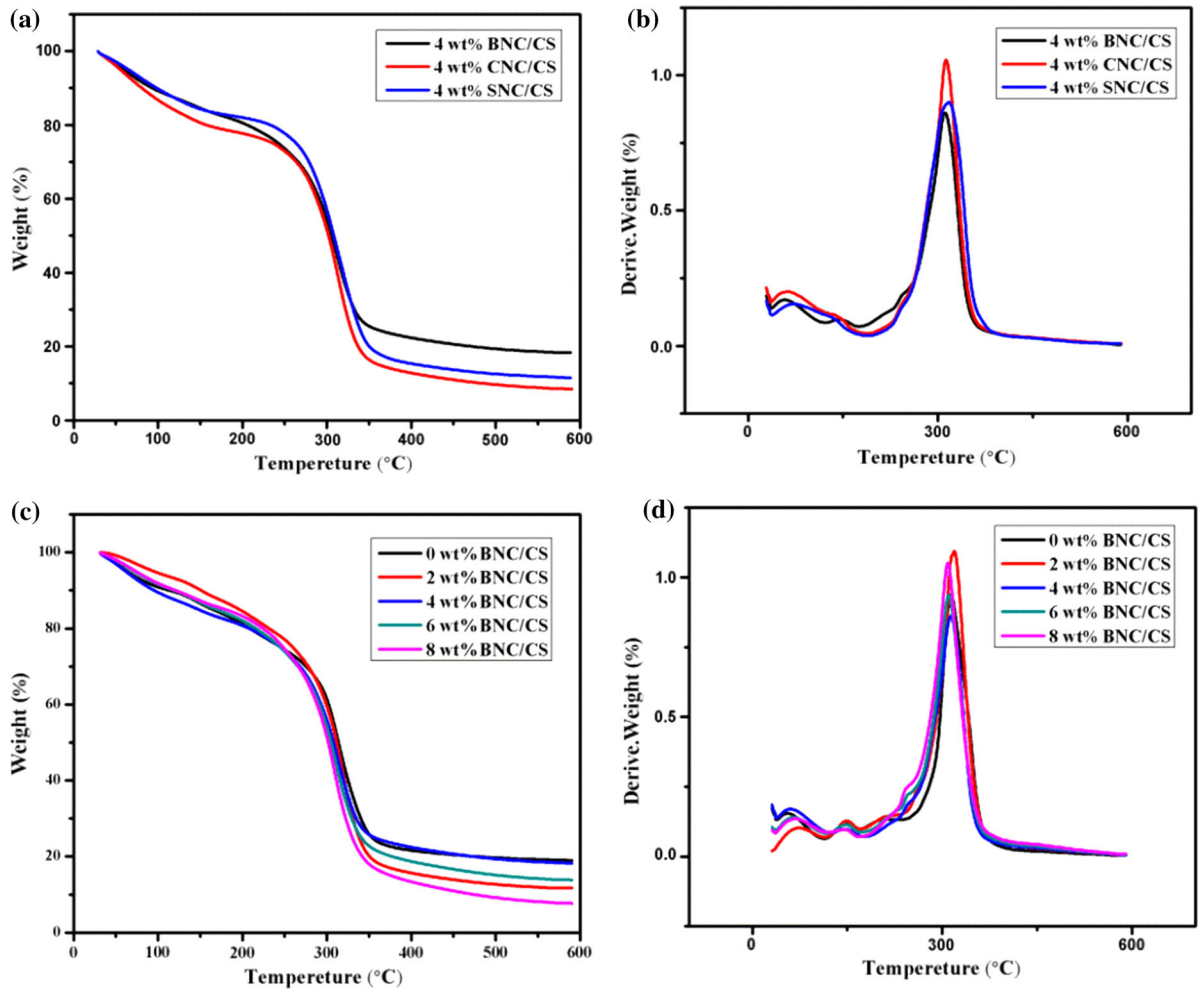

Fig. 7 TG and DTG curves of the composite films

Table 2 Mechanical properties of starch-based composite films reinforced with different contents of BNC, CNC, and SNC respectively

Sample (wt%)	BNC/CS		CNC/CS		SNC/CS	
	TS (MPa)	E (%)	TS (MPa)	E (%)	TS (MPa)	E (%)
0	2.99 ± 0.12	58.71 ± 0.79	2.99 ± 0.12	58.71 ± 0.79	2.99 ± 0.12	58.71 ± 0.79
2	10.56 ± 1.94	35.82 ± 2.63	9.48 ± 0.82	38.93 ± 0.63	4.09 ± 0.64	67.26 ± 5.89
4	12.43 ± 2.70	30.48 ± 1.06	6.82 ± 2.86	37.69 ± 2.39	7.64 ± 1.87	45.47 ± 0.45
6	10.95 ± 1.44	22.33 ± 3.12	10.67 ± 1.54	42.59 ± 1.46	7.45 ± 2.96	26.79 ± 1.36
8	9.14 ± 2.21	22.95 ± 2.69	8.99 ± 2.38	37.25 ± 0.24	7.67 ± 1.64	37.19 ± 2.59
10	9.98 ± 1.32	28.24 ± 2.43	10.28 ± 1.45	23.00 ± 3.51	7.26 ± 0.87	39.10 ± 4.31

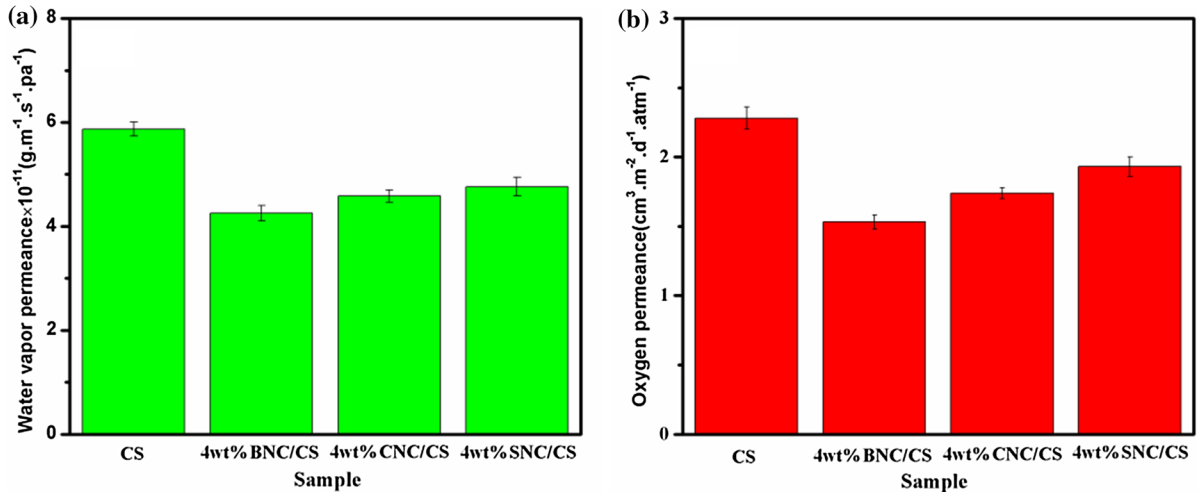

Fig. 8 Water vapor permeation (**a**) and oxygen permeation (**b**) of CS, 4 wt% BNC/CS, 4 wt% CNC/CS, and 4 wt% SNC/CS composite films

increased the curvature and path of the diffusion of water vapor and oxygen.

Conclusions

In this study, three kinds of non-wood nanocellulose were successfully prepared. Moreover, the reinforcing effects of nanocellulose sources and content on starch film were systematically compared. Under the same experimental conditions, the nanocellulose extracted from various sources displayed similar morphology and structure but different size and crystallinity degree. The addition of nanocellulose had no effects on the morphology and transparency of the three kinds of composite films, but the mechanical and barrier properties improved with the addition of nanocellulose. It is worth noting that bamboo nanofibers with the largest aspect ratio had the greatest reinforcing effect on the starch films, although bamboo nanocellulose had the lowest crystallinity degree. This result suggests that the aspect ratio, rather than the crystallinity degree, may be a major consideration when selecting the reinforcing agent for the starch film. Meanwhile, the addition of nanocellulose did not follow a linear pattern of "the more the better"; with the increase of the amount of nanocellulose, the thermal stability and elongation at break of the composite film were reduced, and the tensile force remained unchanged or even weakened after reaching maximum value. As we can see, choosing a suitable raw material and mixed ratio promotes an effective utilization of nanocellulose to achieve the best enhancement for starch film.

Acknowledgments This work was supported by the Science and Technology Project of Guangdong Province (No. 2017B090901064), the Science and Technology Project of Guangzhou (No. 201607020045).

References

Abdul Khalil HP, Davoudpour Y, Islam MN, Mustapha A, Sudesh K, Dungani R, Jawaid M (2014) Production and modification of nanofibrillated cellulose using various mechanical processes: a review. Carbohydr Polym 99:649–665

And MNA, Dufresne A (2008) Plasticized starch/tunicin whiskers nanocomposites. 1. Structural analysis. Macromolecules 33:8344–8353

Babaee M, Jonoobi M, Hamzeh Y, Ashori A (2015) Biodegradability and mechanical properties of reinforced starch nanocomposites using cellulose nanofibers. Carbohydr Polym 132:1–8

Besbes I, Alila S, Boufi S (2011) Nanofibrillated cellulose from TEMPO-oxidized eucalyptus fibres: effect of the carboxyl content. Carbohydr Polym 84:975–983

Bonilla J, Atarés L, Vargas M, Chiralt A (2013) Properties of wheat starch film-forming dispersions and films as affected by chitosan addition. J Food Eng 114:303–312

Carvalho AJF (2008) Chapter 15—starch: major sources, properties and applications as thermoplastic materials. In: Monomers polymers & composites from renewable resources, pp 321–342

Chen J, Long Z, Wang J, Wu M, Wang F, Wang B, Lv W (2017) Preparation and properties of microcrystalline cellulose/hydroxypropyl starch composite films. Cellulose 24:4449–4459

Chirayil CJ, Joy J, Mathew L, Mozetic M, Koetz J, Thomas S (2014) Isolation and characterization of cellulose nanofibrils from *Helicteres isora* plant. Ind Crops Prod 59:27–34

Deepa B, Abraham E, Cordeiro N, Mozetic M, Mathew AP, Oksman K, Faria M, Thomas S, Pothan LA, Universitet LT, Matematik IFRT, Materialvetenskap (2015) Utilization of various lignocellulosic biomass for the production of nanocellulose: a comparative study. Cellulose 22:1075–1090

Faradilla RHF, Lee G, Rawal A, Hutomo T, Stenzel MH, Arcot J (2016) Nanocellulose characteristics from the inner and outer layer of banana pseudo-stem prepared by TEMPO-mediated oxidation. Cellulose 23:1–15

French AD (2014) Idealized powder diffraction patterns for cellulose polymorphs. Cellulose 21:885–896

French AD, Santiago Cintrón M (2013) Cellulose polymorphy, crystallite size, and the Segal Crystallinity Index. Cellulose 20:583–588

García NL, Ribba L, Dufresne A, Aranguren MI, Goyanes S (2010) Physico-mechanical properties of biodegradable starch nanocomposites. Macromol Mater Eng 294:169–177

Jiang F, Hsieh Y (2015) Self-assembling of TEMPO oxidized cellulose nanofibrils as affected by protonation of surface carboxyls and drying methods. ACS Sustain Chem Eng 4:1041–1049

Karimi S (2014) A comparative study on characteristics of nanocellulose reinforced thermoplastic starch biofilms prepared with different techniques. Nord Pulp Pap Res J 29:41–45

Kaushik A, Kaur R (2016) Thermoplastic starch nanocomposites reinforced with cellulose nanocrystals: effect of plasticizer on properties. Compos Interfaces 23:1–17

Kaushik A, Singh M, Verma G (2010) Green nanocomposites based on thermoplastic starch and steam exploded cellulose nanofibrils from wheat straw. Carbohydr Polym 82:337–345

Khalil HPSA, Bhat AH, Yusra AFI (2012) Green composites from sustainable cellulose nanofibrils: a review. Carbohydr Polym 87:963–979

Li M, Li D, Wang LJ, Adhikari B (2015) Creep behavior of starch-based nanocomposite films with cellulose nanofibrils. Carbohydr Polym 117:957–963

Mandal A, Chakrabarty D (2011) Isolation of nanocellulose from waste sugarcane bagasse (SCB) and its characterization. Carbohydr Polym 86:1291–1299

Max J, Chapados C (2004) Infrared spectroscopy of aqueous carboxylic acids: comparison between different acids and their salts. J Phys Chem A 108:3324–3337

Montero B, Rico M, Rodríguez-Llamazares S, Barral L, Bouza R (2016) Effect of nanocellulose as a filler on biodegradable thermoplastic starch films from tuber, cereal and legume. Carbohydr Polym 157:1094–1104

Peressini D, Bravin B, Lapasin R, Rizzotti C, Sensidoni A (2003) Starch–methylcellulose based edible films: rheological properties of film-forming dispersions. J Food Eng 59:25–32

Sacui IA, Nieuwendaal RC, Burnett DJ, Stranick SJ, Jorfi M, Weder C, Foster EJ, Olsson RT, Gilman JW (2014) Comparison of the properties of cellulose nanocrystals and cellulose nanofibrils isolated from bacteria, tunicate, and wood processed using acid, enzymatic, mechanical, and oxidative methods. ACS Appl Mater Interfaces 6:6127–6138

Saito T, Kimura S, Nishiyama Y, Isogai A (2007) Cellulose nanofibers prepared by TEMPO-mediated oxidation of native cellulose. Biomacromolecules 8:2485–2491

Santana JS, Do Rosário JM, Pola CC, Otoni CG, Camilloto GP, Cruz RS (2016) Cassava starch-based nanocomposites reinforced with cellulose nanofibers extracted from sisal. J Appl Polym Sci 134:1–9

Savadekar NR, Mhaske ST (2012) Synthesis of nano cellulose fibers and effect on thermoplastics starch based films. Carbohydr Polym 89:146–151

Segal L, Creely JJ, Martin AE Jr, Conrad CM (1959) Crystallinity of native cellulose using the X-ray diffractometer. Text Res J 10:786–794

Shimizu M, Saito T, Fukuzumi H, Isogai A (2014) Hydrophobic, ductile, and transparent nanocellulose films with quaternary alkylammonium carboxylates on nanofibril surfaces. Biomacromolecules 15:4320–4325

Shinoda R, Saito T, Okita Y, Isogai A (2012) Relationship between length and degree of polymerization of TEMPO-oxidized cellulose nanofibrils. Biomacromolecules 13:842–849

Tabarsa T, Sheykhnazari S, Ashori A, Mashkour M, Khazaeian A (2017) Preparation and characterization of reinforced papers using nano bacterial cellulose. Int J Biol Macromol 101:334–340

Xu X, Liu F, Jiang L, Zhu JY, Haagenson D, Wiesenborn DP (2013) Cellulose nanocrystals vs. cellulose nanofibrils: a comparative study on their microstructures and effects as polymer reinforcing agents. ACS Appl Mater Interfaces 5:2999–3009

Zhao G, Liu Y, Fang C, Min Z, Zhou C, Chen Z (2006) Water resistance, mechanical properties and biodegradability of methylated-cornstarch/poly(vinyl alcohol) blend film. Polym Degrad Stab 91:703–711

Zhou YM, Fu SY, Zheng LM, Zhan HY (2012) Effect of nanocellulose isolation techniques on the formation of reinforced poly(vinyl alcohol) nanocomposite films. Express Polym Lett 6:794–804